LIGHT-INDUCED TRANSFORMATION OF NANOSTRUCTURED $V_3O_7 \cdot H_2O$ TO V_2O_5

By

ÇAĞRI ÖZGE TOPAL

Bachelor of Science in Mechanical Engineering

Dokuz Eylül University

Izmir, Turkey

2006

Submitted to the Faculty of the
Graduate College of the
Oklahoma State University
in partial fulfillment of
the requirements for
the Degree of
MASTER OF SCIENCE
May, 2010

LIGHT-INDUCED TRANSFORMATION OF

NANOSTRUCTURED $V_3O_7 \cdot H_2O$ TO V_2O_5

Thesis Approved:

Dr. A. Kaan Kalkan

Thesis Adviser

Dr. Raman P. Singh

Dr. Sandip P. Harimkar

Dr. A. Gordon Emslie

Dean of the Graduate College

ACKNOWLEDGMENTS

First and foremost, I would like to express my gratitude to my adviser, Dr. A. Kaan Kalkan, for his patience, encouragement, and warmhearted guidance and support throughout my Masters studies. I am grateful to him for inspiring me by his endless enthusiasm, and passion for science and research. I would also like to thank to the members of my thesis committee Dr. Raman Singh and Dr. Sandip Harimkar for their valuable time, and feedback.

I would like to extend my sincere thanks to Dr. Hongbing Lu, Dr. Nicholas Leventis, and Gitogo Churu for providing us with information on vanadium oxide aerogel preparation technique. I would also express my gratitude to Dr. Jay Hanan, Dr. Alejandro Rodríguez Navarro from University of Granada in Spain and Masoud Allahkarami for their help on X-Ray diffraction studies.

I want to express my acknowledgements to Dr Susheng Tan and Terry Colberg for their help on SEM. My sincere thanks also go to the members of the Functional Nanomaterials Laboratory for their friendship and support.

Finally, I would like to thank to my parents, my brother, my sister and my boyfriend for their unflagging understanding, support, encouragement and love.

TABLE OF CONTENTS

LIST OF FIGURES

CHAPTER 1

INTRODUCTION

Transition metals are the elements with incomplete d electron shells. One interesting attribute of transition metals is that they exhibit variety of oxidation states. Consequently, they can form several single valence, and mixed valence oxides. Due to this diversity in chemistry, transition metal oxides can exhibit chemical and structural transformations under the influence of different external factors, such as electron and ion bombardment, heat treatment, and electromagnetic radiation [1]. Further, transition metal oxides have the ability to influence the reduction and oxidation processes finding uses as catalysts, and catalytic supports [2]. Transition metal oxides also serve as electrode materials in certain electrochemical devices. In addition, they are utilized in electronics industry as transparent conducting oxides or active semiconductor layers [3].

In the present thesis work, light induced phase transformation of a transition metal oxide has been observed and studied. This phase transformation occurs between two different oxides of vanadium, prepared by sol-gel chemistry, namely from $V_3O_7 \cdot H_2O$ to V_2O_5, under laser irradiation as low as $\cong 0.31$ kW/cm^2. An interesting feature of this phase

transformation is found to be its athermal origin.

Some of the vanadium oxides, such as VO_2 and V_6O_{13}, undergo a metal to semiconductor phase transition involving change in crystal structure at certain temperatures. This property of vanadium oxides provides an opportunity for numerous electrical and optical applications, such as optical and electrical switches, optical memory, thermistors, and reflectors [4-6].

In addition, amorphous to crystalline transition in V_2O_5 was reported by Witke *et al.* by a 514.5 nm argon ion laser at 63.6 kW/cm^2 power density. The same group also demonstrated laser induced oxidation of V_4O_9 to V_2O_5 by 514.5 nm laser irradiation of 190.8 kW/cm^{-2}. They attributed this transformation to a thermal effect [7]. Further, Liu *et al.* observed laser induced coloration of V_2O_5 (i.e., from pink yellow to dark blue) upon 308 nm XeCl excimer laser irradiation of 3.47×10^6 W/cm^2. They attributed this coloration to a laser induced creation of defects (i.e., thermochromism) [8].

The present wok investigates the light induced $V_3O_7 \cdot H_2O$ to V_2O_5 transformation by Raman spectroscopy. This investigation was carried out in both air and Ar ambient. Raman spectroscopy was also employed to rule out the heating effects and measure the temperature during this transformation which is as low as 25-29 °C (i.e., measurements performed at room temperature). In contrast, it is observed by Zakharova *et al.* that the same transformation occurs at 400 °C when it is driven thermally by annealing samples for 30 minutes [9]. Further, the present work explored kinetics of the light-induced $V_3O_7 \cdot H_2O$ to V_2O_5 transformation by photoluminescence.

The organization of the present thesis is as follows. In Chapter 2, the background on properties and certain applications of vanadium oxides is reviewed. In Chapter 3, procedures for vanadium oxide aerogel preparation and characterization methods utilized are described. Chapter 4 presents the results. In particular, Raman scattering was used to monitor the phase transformation and measure the temperature during the transformation. In addition, the kinetics of the phase transformation as probed by photoluminescence is discussed. Electron microscopy images and X-ray diffraction data are provided for the elucidation of nanostructure and crystal structure. Finally, Chapter 5 concludes the present study, and suggests directions for future research.

CHAPTER 2

BACKGROUND

Vanadium is a transition metal which is found in several different minerals, iron ores, as well as in crude oil deposits. V was first discovered by A.M. del Rio, a Spanish mineralogist, in 1801 and named as erythronium. The element then was declared and had been known as an impure form of chromium until it was rediscovered in 1830 by Swedish chemist N.G. Sefström. Sefström named this new element vanadis, the nick name of Scandinavian fertility and love goddess Freyja [10, 11].

Vanadium has different variety of metallurgical applications. A most common application of vanadium is as an additive to improve shock and vibration resistance of steel. Vanadium also finds wide applications in aerospace industry in, such as jet engines and high-speed airframes. When mixed in titanium alloys with aluminum, vanadium increases titanium's strength, and resistance to high operating temperatures and stress. In addition, vanadium salts are used in ceramics and textile dyes due to their bright colors [11].

Vanadium exhibits main oxidation states of +2, +3, +4 and +5 in its oxides with variety of crystal structures. There are four single valence oxides of vanadia which

consist of ions with the same valence charge, VO, V_2O_3, VO_2, and V_2O_5. In addition, there are certain oxidation states of vanadia where ions of different valence charges present at the same time called mixed valence oxides. Examples of these oxides are V_nO_{2n-1} and V_nO_{2n+1} Magneli phases with $2 \leq n \leq 9$ [12]. Due to this diversity in chemistry, vanadium oxides offer physical, chemical, and electronic properties which find use in a wide range of applications in, such as gas sensors, lithium insertion electrodes, catalysts and optical switches [13-15].

Vanadium oxides are generally used as catalysts. Typically, vanadium oxides are used to catalyze certain oxidation processes, such as oxidation of SO_2 to SO_3, naphthalene or *ortho*-xylene to phthalic anhydride, and n-butane to benzaldehyde. In recent years, vanadium oxide catalysts also have been used in the reduction of NO_x [11, 16]. Besides oxidation and reduction of various chemicals, this group of catalysts is also exploited in gas sensing. As an example, reducing gases such as SO_2 and hydrocarbons can be detected by vapor deposited V_2O_5 films on the basis of electrical conductivity change [17].

V_2O_5 is an attractive material as a counter electrode for Li batteries due to its low cost, high energy density, easy synthesis, and high stability. The performance of V_2O_5 cathodes highly depends on the crystallinity. Consequently, there have been many studies on improving the performance of these cathodes (e.g., better specific capacity and cyclability) by modifying the structure. A number of studies have shown that crystalline V_2O_5 cathodes exhibits high specific capacity, but the cyclability is substantially weak because of the structural damage during the cycles. However, amorphous and low crystalline V_2O_5 have high Li-ion diffusion rate, and significant cyclability [18].

Morphology is another important parameter for the performance of the cathode materials. Lately, nanostructured cathode materials have become popular owing to their enhanced capacity and cyclability. This enhancement in performance results from size effects including high surface to volume ratio, and changes in the energy distribution of electronic states. In particular, highly porous nanostructures, e.g., aerogels, would be ideal candidates as the cathode for high performance Li batteries, because the electrolyte would easily penetrate into the material, and also the distance which the intercalated ions travel is reduced [18, 19].

Vanadium oxides can exhibit different electronic properties. Some of the vanadium oxides show metallic characteristics, such as V_2O_3 and V_7O_{13}, whereas some of them are semiconductors, such as V_2O_5, V_3O_7, and V_4O_9. In addition, some of the vanadium oxides undergo a reversible metal to semiconductor phase transition. Examples of these oxides are VO_2, and V_6O_{13} which exhibit metal to semiconductor phase transition at 340 and 150 K, respectively [4]. The metal to semiconductor transition in vanadium oxides occur along with a change in crystal structure. For example, crystal structure of VO_2 changes from monoclinic to tetragonal while it transforms from semiconductor to metal [4]. Besides a change in the electronic properties, a dramatic change in optical properties also occurs through this phase transformation that opens the door to optical switching [5].

Another attractive property of the vanadium oxides are the photochromism, and electrochromism. Photochromism, or electrochromism is the ability of a material to change its optical absorption when exposed to an optical excitation, or an electric field [20, 21]. After the exposure is removed, the coloration remains, but it can be reversed

when another optical source, or reversed electric field is applied. This feature of vanadium oxides makes them proper candidates in applications, such as information displays, and optical switches [21].

The reason behind the coloration of these materials is the trapping of electrons in certain lattice sites (i.e., midgap electronic states) that changes the visible light absorption of the material. In the photochromic case, these trapped electrons are provided internally from the material itself (i.e., valence band). However, in the case of electrochromism, electrons are provided externally by an applied electric field [21].

In addition to photochromism and electrochromism, coloration in vanadium oxides can occur due to a photo-induced thermochromism [20]. Laser induced coloration, crystallization, and oxidation of certain vanadium oxides have been studied by different groups [7, 8, 22]. Liu *et al*. demonstrated laser-induced coloration of V_2O_5 pellets under 308 nm XeCl excimer laser with 3.47×10^6 W cm^{-2} energy density. They showed that samples were changed color from pink yellow to dark blue along with an increase in conductivity. Originally, V_2O_5 is a semiconductor at room temperature, whereas the colored samples have electrical resistivity in the order of 10^3 Ωcm. They attributed this coloration to a laser induced thermochromism. In their X-ray diffraction and Raman spectroscopy measurements, they observed that the samples were sub-stoichiometric with an oxygen deficiency, but the crystalline structure was the same as the uncolored samples [8].

In another study, Witke *et al.* showed the laser-induced crystallization of potentiodynamically produced amorphous vanadium oxide thin films by a 514.5 nm

argon ion laser at 63.6 kW/cm^2 power density. In the same study, they also demonstrated laser-induced oxidation of V_4O_9 thin films with addition of V_2O_5 phase to V_2O_5 at 190.8 kW/cm^2 power density [7].

There are several vanadium oxide hydrates consisting of +5 and +4 oxidation states. $V_3O_7{\cdot}H_2O$ is one of the most attractive oxides in this group of materials due to its promising electrochemical and catalytical properties. In particular, different types of nanostructured $V_3O_7{\cdot}H_2O$, such as nanobelts, nanofibers, and nanowires, have received great attention, and their structures and electrochemical properties have been studied [9].

As described by Oka *et al.*, structure of vanadium oxide hydrate is layered consisting of two types of VO_6 octahedra (V(1) O_6 and V(2) O_6) and one type of VO_5 trigonal bipyramid. In this structure, a V(1) O_6 and a V(2) O_6 octahedron share edges, and form piles along the *c* axis. Further, two VO_5 trigonal bipyramids sharing edges along the *b* axis connect theseVO_6 piles and form V_3O_8 layers along the *a* axis (Fig. 2.1a). The V_3O_8 layers are hold together by water molecules which replace one of the oxygen atoms in a VO_6 octahedron in one layer and form hydrogen bond with a VO_6 octahedron in another layer [9, 23]. According to our understanding, water molecule is bound to a VO_6 octahedron by forming a coordinate bond between oxygen and vanadium where the shared electrons come from oxygen as shown in Fig. 2.1b. This model explains how a vanadium atom can make bonds with six oxygen atoms while its highest oxidation state is +5.

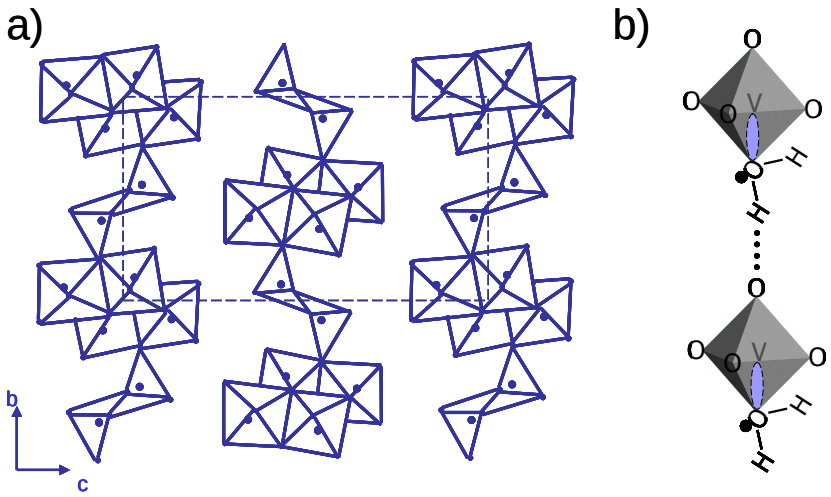

Figure 2.1: a) Crystal structure of $V_3O_7 \cdot H_2O$. The sketch is inspired from Oka *et al.* [23]. The dots represent V atoms. **b)** Model illustrating the coordinate bonds between vanadium and oxygen in water. The model also shows how V_3O_8 sheets are hold together by hydrogen bonds.

V_2O_5 has a structure similar to $V_3O_7 \cdot H_2O$. It is orthorhombic with a corrugated sheet type (layered) structure at room temperature. The basic unit is a distorted trigonal bipyramid in which vanadium atom is surrounded by three types of oxygen; vanadly (O^1), chain (O^2), and bridge (O^3). In this basic unit, due to the distinct displacements of vanadium atoms in [VO_6] octahedron, the basic unit turns into VO_5 square pyramid as seen Fig. 2.2. The sheet structure is formed by these distorted bipyramids sharing edges and corners [24]. Further, V_2O_5 is yellow-orange colored with a band gap of 2.2-2.3 eV as reported by different groups [25, 26].

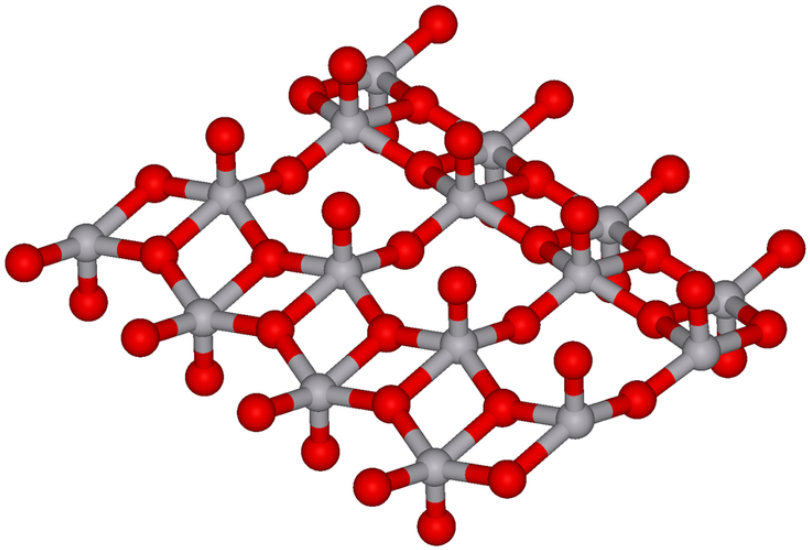

Figure 2.2: V_2O_5 crystal structure (the copyright holder of this work releases it into the public domain; http://en.wikipedia.org/wiki/File:Vanadium-pentoxide-monolayer-3D-balls.png , January 7, 2010).

CHAPTER 3

METHODOLOGY

3.1. Materials and Sample Preparation

3.1.1. Precursor Materials

Vanadium (V) tripropoxide (VO ($OCH_2CH_2CH_3)_3$) was purchased from Sigma Aldrich, Inc. Acetone (HRGC/HPLC grade) was purchased from Pharmco-AAPER Alcohol and Chemical, Inc. Both chemicals were used as received. Deionized water (18.2 MΩcm) was obtained from an Elga Purelab Ultra water purification system. Siphon grade CO_2 was purchased from Stillwater Steel and Supply, LLC, Stillwater, OK.

3.1.2. Synthesis of Aerogels

In the present study, $V_3O_7 \cdot H_2O$ aerogels were prepared by supercritical drying of wet vanadia gels obtained via modification of Dunn's procedure as indicated in the paper of Leventis *et al.*[27] In this process, a mixture of 5.58 ml of deionized water and 11.34 ml of acetone was added to 2.4 ml of vanadium(V) tripropoxide, $VO(OCH_2CH_2CH_3)_3$.

In order to slow down the gelation process, the liquid precursors (i.e., as described above) were cooled in a CO_2 ice/acetone bath (-78 °C) until ice appeared in water/acetone

mixture and vanadium (V) tripropoxide became more viscous. Prior to the mixing, water/acetone mixture was shaken vigorously until ice chunks disappeared. The water/acetone mixture was subsequently added into vanadium (V) tripropoxide at once. The obtained mixture (sol) was shaken for 10-15 seconds and transferred to the polyethylene syringes (Becton Dickinson & Co., Luer-LokTM Tip, 5 ml) immediately while it was still cold, and sealed with Parafilm. Samples were aged for five days in their molds (syringes). After aging, gels were removed from the syringes and placed into a jar filled with anhydrous acetone, approximately 4-5 times the total gel volume. The acetone was changed periodically, once every 24 hours for four times. After the water inside the aerogels was fully exchanged with acetone, supercritical drying with CO_2 was performed to remove the acetone. Figure 3.1 shows the preparation steps of vanadium aerogels.

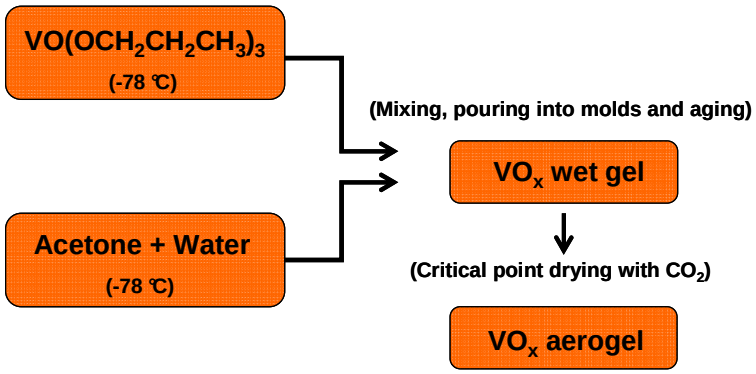

Figure 3.1. Schematics of vanadia aerogel preparation.

3.1.3. Critical Point Drying of Aerogels

Drying process is the most critical step in the aerogel preparation. Aerogels prepared by the method described in Section 3.1.2 are highly porous and fragile [27]. Drying of samples in air, results in collapse of the pores due to the capillary forces.

Therefore, the acetone in the aerogel was removed by critical point drying (CPD) without any damage to the structure.

As the liquid evaporates, the samples are subject to capillary forces present at the phase boundary. However, at critical point, a fluid and its vapor phase coexist and the surface tension between these two phases becomes zero. If the temperature and the pressure are kept above the critical point, super critical fluid can be released without harming the structure of the samples [28].

In the present study, critical point drying of aerogels was performed by Quorum Technologies E3100 Series critical point dryer. Samples were placed on the sample holder of the dryer, and the sample holder was placed into the pressure chamber of the system. The system was pre-cooled to 20 °C by running cold water. In order to prevent air drying, the dryer chamber was filled with acetone initially. Subsequently, the access door was closed tightly, and the supply valve of the gas cylinder was opened. The inlet valve was opened fully to fill the chamber with liquid gas. Samples were left in the liquid CO_2 for 20 minutes to allow the penetration of the liquid CO_2 into the samples. The substitution liquid was then drained through the drain valve. This flushing step was repeated for 8-10 times until the acetone was completely replaced with liquid CO_2.

Subsequent to the flushing steps, the chamber was filled with liquid CO_2 until the liquid reached to the top of the chamber. At this point, temperature of the liquid CO_2 was around 18 °C , and the pressure inside the chamber was approximately 955 Psi (65 Atm). The inlet valve was closed and the hot water supply was turned on to increase the temperature of the chamber. The chamber was observed through the viewing window,

while the temperature and pressure gauges were being monitored. After CO_2 reached to its critical point (31.1 °C and 1072 Psi), the temperature was kept constant at around 40 °C while the pressure was maintained at 1200 Psi. The samples were left in the super critical CO_2 for 2 hours. After 2 hours, the vent valve was opened slowly (around 3-4 hours venting time) to vent the gas inside the chamber, and the samples were removed from the chamber.

Figure 3.2 shows the phase diagram of CO_2. In this phase diagram, A indicates the point where the chamber is filled with liquid CO_2 (around 18 °C and 955 Psi). After heating the chamber, CO_2 passes the critical point and reached to the point B (40 °C and 1200 Psi). Finally, CO_2 is vented while the temperature is constant at 40 °C, and the drying process is complete (point C).

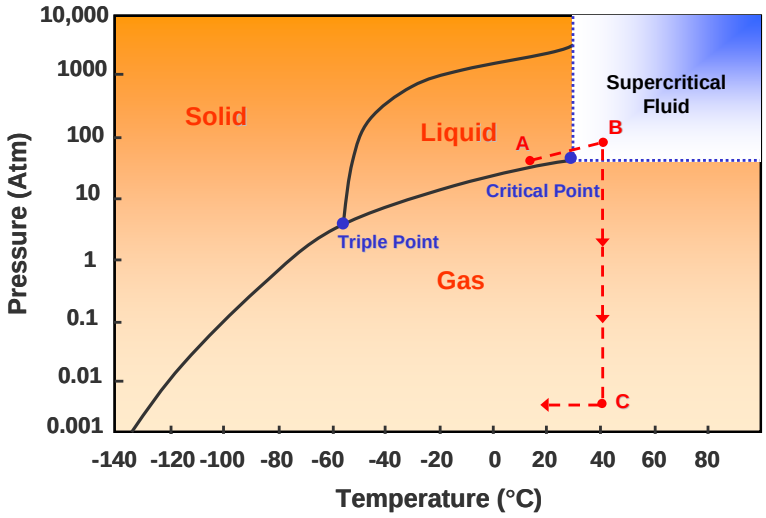

Figure 3.2: Pressure - temperature phase diagram of CO_2.

3.2. Laser Exposures and Raman Scattering Measurements

Raman scattering, a spectroscopic method based on inelastic scattering of photons, was first observed by C. V. Raman in 1928. Since Raman spectrum of a substance provides characteristic information about the molecular and crystal structure, Raman scattering has been widely used for identification of molecules and materials [29].

When light interacts with matter, photons can either pass through without interacting with the material or can be scattered or absorbed [30]. Most of the scattered photons experience no change in energy (i.e., elastic scattering) that is known as Rayleigh scattering. However, in the Raman scattering, the incident light is scattered inelastically, where the scattered photon loses or gains energy to/from a vibrational mode; i.e., phonon. As illustrated in Fig. 3.3, in light scattering, the incident light first excites an electron from a ground state to a virtual state. If the electron subsequently turns back to the same ground state, a photon is emitted having the same energy as the incident photon. This event is the Rayleigh scattering. However, the excited electron may relax to a vibronic state, which represents the coupling of the ground state with a vibrational mode, as seen in Fig. 3.3. In this case, the emitted photon has less energy than the incident photon by the energy of the vibrational mode. In the language of quantum mechanics, a phonon is created. This type of Raman scattering is called Stokes Raman scattering. On the other hand, as illustrated in Fig. 3.3, the electron may also be excited from a vibronic state and relax to the ground state. In this case, the emitted photon has higher energy than the incident one by an amount equal to that of the phonon. Equivalently, a phonon is annihilated transferring its energy to the photon. This event is called anti-Stokes Raman scattering [31].

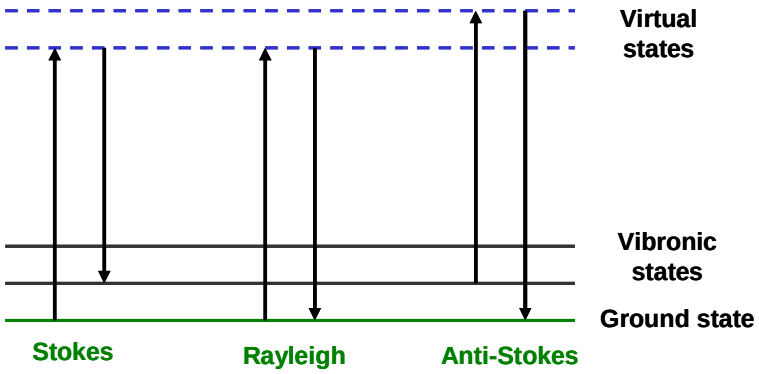

Figure 3.3. Energy diagram illustrating Rayleigh and Raman scattering.

In the present study, a Renishaw RM 1000 micro Raman system equipped with a CCD camera and Leica DMLM microscope was used for conducting and monitoring of the phase transformation. Raman scattering acquisitions were performed by an 1800 lines/mm grating. A Spectra-Physics 160-series Ar^{+} laser of 514 nm was used as the excitation source. The system was calibrated with a (111) silicon wafer with reference to the 1^{st} order Raman scattering peak of Si at 520.5 cm^{-1}.

For Raman scattering scans of vanadium aerogels, samples were placed on a microscope slide and all measurements were performed at room temperature in the dark. A 20× objective lens with numerical aperture of 0.4 was manually focused on the samples. The laser beam was defocused by 20% to disperse the irradiation over an area of 16.2 μm diameter.

First, the Raman spectrum of a vanadia aerogel sample was collected under 0.6 mW incident laser power at an accumulation of 200 seconds. Subsequently, the incident laser power was increased to 6mW at which the transformation of the material occurs, and a new spectrum was collected under the same conditions. After transformation,

during which the second spectrum was collected, the power was decreased to its initial value (0.6 mW), and another Raman scan performed and recorded.

3.3. Temperature Measurement by Raman Spectroscopy

Besides molecular or materials identification, Raman scattering may also be used as a sensitive tool for temperature measurement [6, 7]. For a given vibrational mode, the ratio of anti-Stokes Raman scattering intensity to Stokes Raman scattering intensity is a Boltzmann factor, from which the temperature can be derived. This relation is given by

$$\frac{I_{as}}{I_s} = e^{-E_p/kT} \tag{1}$$

which is essentially the Boltzmann distribution function, where,

I_{as}= Intensity of the anti-Stokes line

I_s= Intensity of the Stokes line

E_p = Phonon energy (i.e., Raman shift)

k = Boltzmann constant (1.38×10^{-23} J/K)

T = Temperature (K)

Here the photon energy E_p was calculated by using the relation:

$$E_p = \frac{hc}{\lambda} \tag{2}$$

where,

hc=1.24 eV×μm (h is the Planck's constant and c is the speed of light),

1/λ= wavenumber of the Raman peak.

In the present study, the temperature at which the $V_3O_7{\cdot}H_2O$ to V_2O_5 phase transformation of vanadium aerogels occurs was measured by Raman scattering. Since the $V_3O_7{\cdot}H_2O$ anti-Stokes peaks yield poor signal to noise ratio, $V_3O_7{\cdot}H_2O$ was first partially transformed to V_2O_5 at around the transformation threshold laser intensity. Typically, the transformation was driven to ~33% completion. At around the threshold laser intensity, the transformation can be slowed down and a mixed phase can be obtained controllably. Then, the temperature measurement was based upon Stokes and anti-Stokes peaks of the V_2O_5 phase, which yields significantly sharper Raman peaks at higher signal to noise, as will be disclosed in Chapter 4. Once the transformation is significantly slow, V_2O_5 phase is in thermal equilibrium with the $V_3O_7{\cdot}H_2O$ phase. Therefore, the temperature calculation was based on Stokes and anti-Stokes peaks of the V_2O_5 phase.

In order to find the lowest laser power (i.e., threshold) at which the phase transformation occurs, and the two phases coexist, the laser beam was focused on the samples by a 20× objective lens where the laser spot size on the sample was adjusted to 33.3 μm. Raman scattering was performed under different laser powers, until the lowest incident power level, at which the Raman peaks associated with V_2O_5 appear in the spectrum. This power threshold was found to be 2.66 mW. Thus, temperature measurement was performed by collecting Stokes and anti-Stokes peaks separately with

the 20× objective lens under 2 mW incident power at an accumulation of 200 seconds. Intensities of the Stokes peaks at 405 and 283 cm^{-1} and the anti-Stokes peaks at -405 and -283 cm^{-1} for V_2O_5 were used for the calculation of transformation temperature.

3.4. Raman Acquisitions in Argon Ambient

In order to investigate the $V_3O_7.H_2O$ to V_2O_5 transformation in an inert environment (e.g., oxygen-free and water-free), samples were enclosed in septum-sealed optical cells, which were subsequently purged with argon gas. Two syringe needles were pierced into the septum; one for gas intake which was connected to the argon cylinder, and the other for gas exit which was open to the atmosphere. Argon pressure was kept at around 1 psi to allow a laminar flow without harming the sample, while the original air inside the cell was purged off through the other needle. Samples were purged for at least 10 minutes. At the end of the purging, the needle open to the atmosphere was removed first.

The Raman scattering of the sample kept in argon was performed with 20× objective lens (numerical aperture of 0.4). The laser beam was defocused by 20% to disperse the irradiation over an area of 16.2 μm diameter.

3.5. Electronic Band Gap Calculation

To the best of the author's literature search, no information is available on the electronic and optical properties of $V_3O_7{\cdot}H_2O$. Accordingly, optical absorption scans were carried out to estimate the electronic band gap of $V_3O_7{\cdot}H_2O$. Since, the sol-gel synthesized vanadia samples are opaque and they cannot be cleaved to thin films due

their extreme fragileness, measurements were performed with samples dissolved in deionized water at a concentration of 3.4 g/l. Cary 300, a double beam spectrophotometer was employed to measure the optical transmission using deionized water as the reference. Both the water reference and the vanadia sample were enclosed in Starna UV-Vis optical cells. The transmission coefficient (T) was converted to absorbance (A) as

$$A = -\log(T) \tag{3}$$

From which the band gap was derived as will be discussed in Chapter 4.

3.6. Transformation Kinetics by Photoluminescence

The $V_3O_7.H_2O$ to V_2O_5 transformation kinetics was monitored from the intensity of V_2O_5 photoluminescence (PL) in time series, where $V_3O_7.H_2O$ essentially exhibits no PL, while V_2O_5 has a broad emission under 514.5 nm excitation. Renishaw RM 1000 micro Raman system was employed for the PL acquisitions. All PL measurements were performed by a 150 lines/mm grating using a 20× objective lens (0.4 numerical aperture) in time series, acquiring a spectrum at every 2 seconds (1 second excitation time) , for a total of 100 secons at 0.8 mW incident laser power. The laser irradiation was dispersed over an area of 16.2 μm diameter by defocusing the laser beam by 20%.

CHAPTER 4

RESULTS AND DISCUSSION

4.1. Physical Characterization of Samples

Vanadium aerogels were prepared as described in Sections 3.1.2 and 3.1.3. During the preparation process the water/acetone solution, vanadium (V) tripropoxide and precursor solution were cooled in order to prevent quick gelation. The obtained samples were dried by supercritical drying with liquid CO_2 as described in Section 3.2. Supercritical drying of aerogels allows slow extraction of acetone from gels and prevents the collapse of the structure due to the capillary forces. The synthesized wet-gels had a reddish color before the aging process. During the aging, the color of aerogels changed to brown and finally to dark green (Fig. 4.1).

Structure of the vanadia aerogels was studied by a FEI Quanta 600 field-emission scanning electron microscope (SEM). SEM image in Figure 4.2 shows that the structure of vanadia aerogels consists of 15 to 20 nm diameter, and microns long nanowire building blocks.

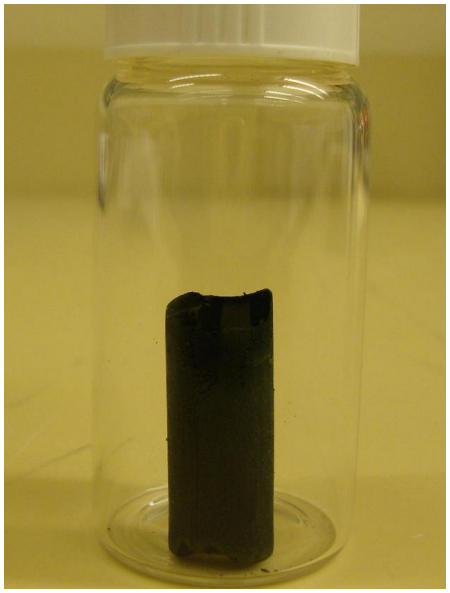

Figure 4.1: Sol-gel synthesized $V_3O_7 \cdot H_2O$.

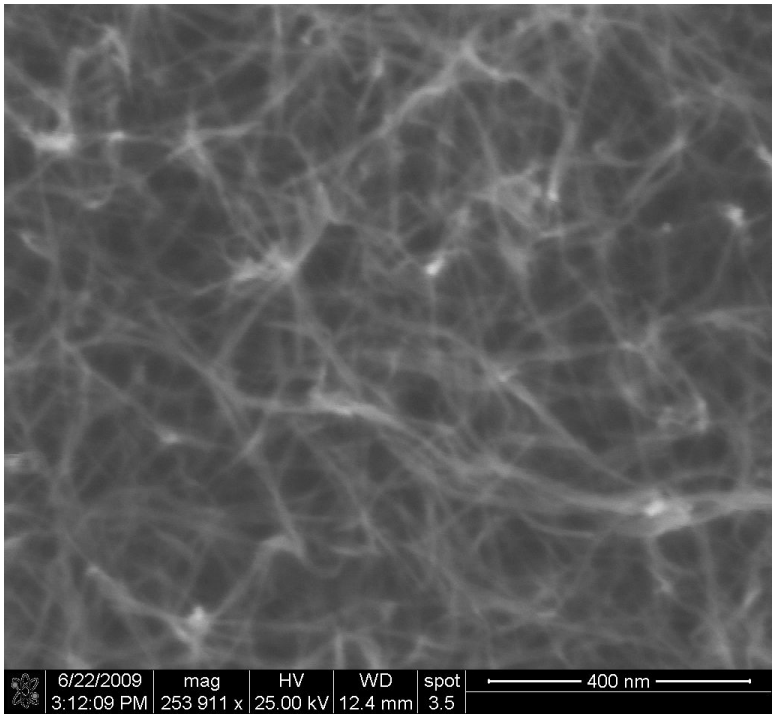

Figure 4.2: SEM image of sol-gel synthesized $V_3O_7 \cdot H_2O$.

Aerogel samples were also characterized using PanAnalytical XPert X-ray Powder diffractometer with a Pixel detector using Cu K_α (0.152 nm) radiation. Figure 4.3. shows the X-ray diffraction (XRD) spectrum of a typical aerogel sample. The diffraction peaks reveal a nanocrystalline material. The optimal fit for the observed X-ray spectrum was found to be orthorhombic $V_3O_7 \cdot H_2O$ (trivanadium pentaoxide hydrate) [34]. In addition, the XRD spectrum as well as its assignment are in agreement with the previous work of Leventis *et al.* [27]. Further, their XPS findings revealed that the vanadium is present as vanadium(V) and vanadium(IV) at fractions of 67.61% and 32.39%, respectively.

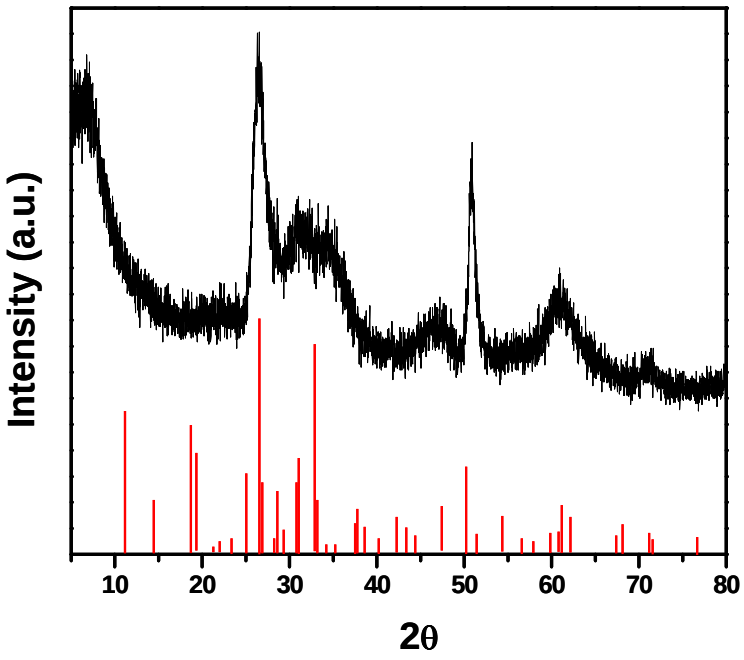

Figure 4.3: XRD spectrum of a vanadium oxide aerogel sample. The line spectrum represents $V_3O_7 \cdot H_2O$ for comparison (JCPDS-85-2401).

Finally, vanadia aerogels were characterized by Raman scattering as described in Section 3.2. Figure 4.4.a shows the Raman spectrum of a typical vanadia aerogel.

4.2. Laser Induced Phase Transformation of Vanadia Aerogels at 514 nm

During the Raman scattering acquisitions, we discovered a phase transformation of the $V_3O_7.H_2O$ aerogel to V_2O_5 under 514nm laser above a certain threshold laser intensity. The phase transformation was clearly monitored from the dynamic Raman spectrum of the sample under excitation.

Figure 4.4.a shows the Raman spectrum of vanadia aerogels before the transformation at 0.29 kW/cm^2 incident laser intensity. On the other hand, Figure 4.4.b is the Raman spectrum collected with ten times the laser intensity; i.e., 2.9 kW/cm^2. Obviously, the higher laser intensity spectrum is different indicative of a phase transformation or chemical reaction. The captured Raman spectrum during this transformation is dominantly characteristic of V_2O_5. After the material is fully transformed, a final Raman spectrum of the aerogel was collected at 0.29 kW/cm^2 incident laser intensity that is provided in Fig. 4.4.c. As can be seen in Fig. 4.4, there is also a reduction in the background of the Raman spectrum. In view of Raman scattering literature, this new phase is identified as crystalline V_2O_5 [35].

The assignments of Raman peaks in spectrum of V_2O_5 are as follows. The mode at 995 cm^{-1} is V═O stretching. The 703 cm^{-1} peak corresponds to V─O stretching of doubly coordinated oxygen (associated with the corner shared oxygens). The 527 cm^{-1} mode is the V─O stretching from triply coordinated oxygen (associated with the edge-shared oxygen). The mode at 483 cm^{-1} is the bending vibration in V─O─V groups. The

405 and 283 cm^{-1} peaks are due to the V═O bending, and finally, 196 and 145 cm^{-1} are the lattice vibrations due to the layered structure of V_2O_5 [36, 37].

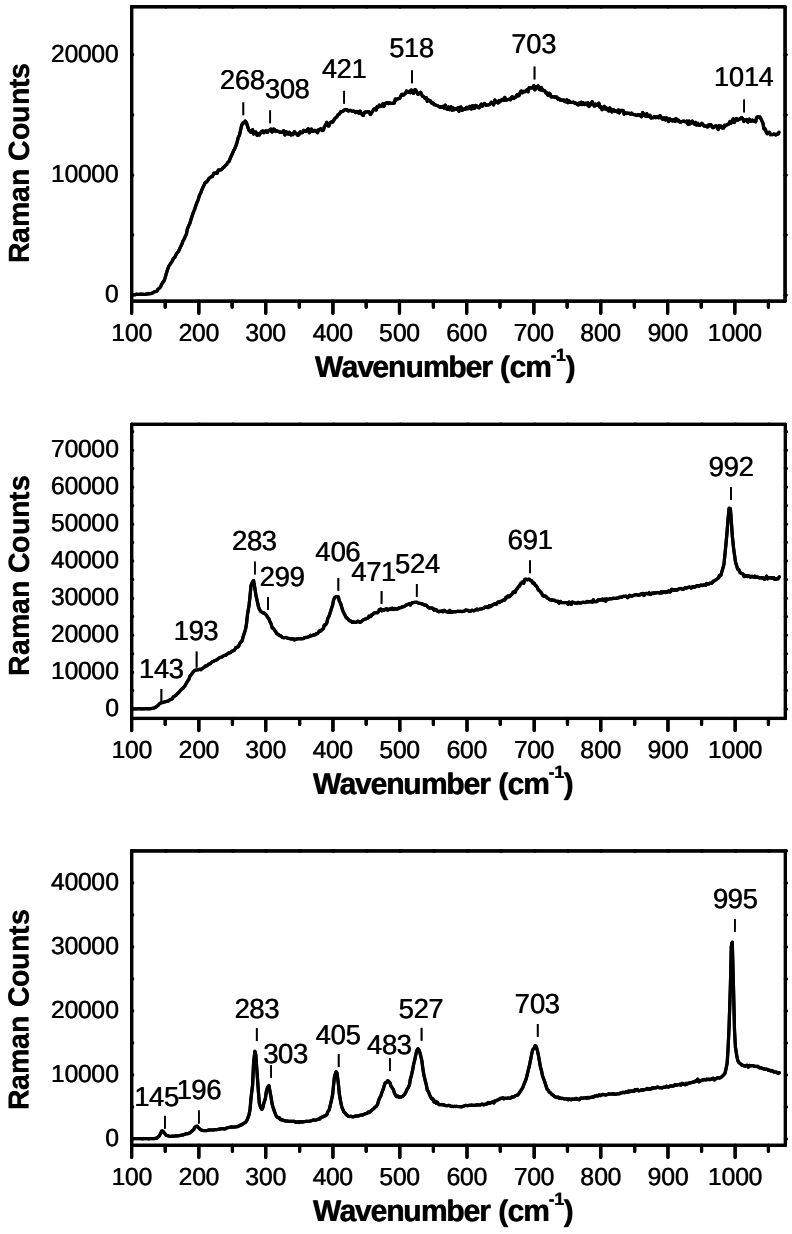

Figure 4.4: Raman spectra of vanadia aerogel sample: **a)** $V_3O_7 \cdot H_2O$ before laser exposure at 0.29 kW/cm^2 intensity; **b)** vanadia, which was originally $V_3O_7 \cdot H_2O$ but immediately transformed to V_2O_5 during Raman scan (200 s) at 2.9 kW/cm^2 laser

intensity **c)** transformed material (V_2O_5) after laser exposure as in (b) However, 0.29 kW/cm^2 laser intensity was employed for the Raman acquisition.

As seen in the optical micrograph of Fig. 4.5, a distinct color change was observed at the spot, which was exposed to the laser. This color change is attributed to the phase transformation to V_2O_5. Further, during the transformation, the scattered laser radiation from the spot (after attenuation by a factor of 100) was captured in a video. Typically, the image of the scattered laser from the sample surface is observed as an interference pattern with an ensemble of bright spots. Interestingly, random blinking of these spots was observed during the course of the transformation indicative of structural changes on the surface. Eventually, this blinking ended implying the completion of the transformation. The laser transformed region was also examined by SEM as shown in Fig.4.6. It is observed that the transformed V_2O_5 region has undergone a volumetric contraction and increase in density of vanadia wires.

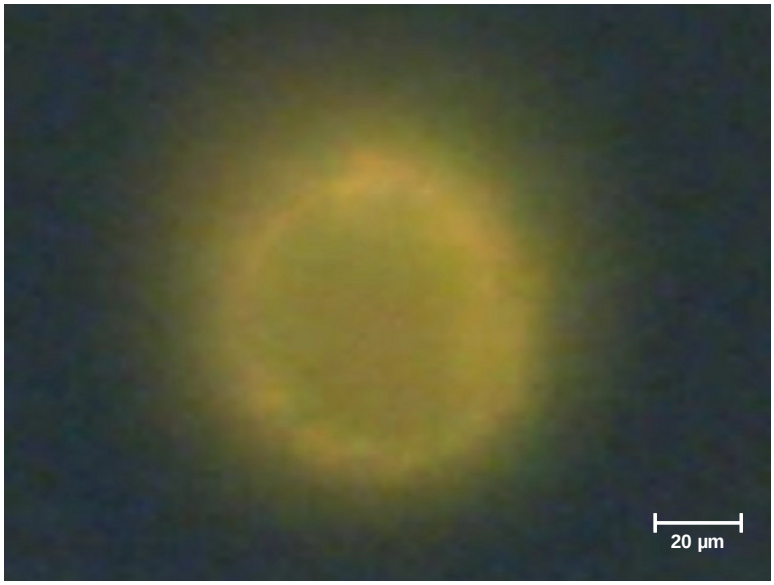

Figure 4.5: Optical image showing laser exposed region of a typical vanadia aerogel.

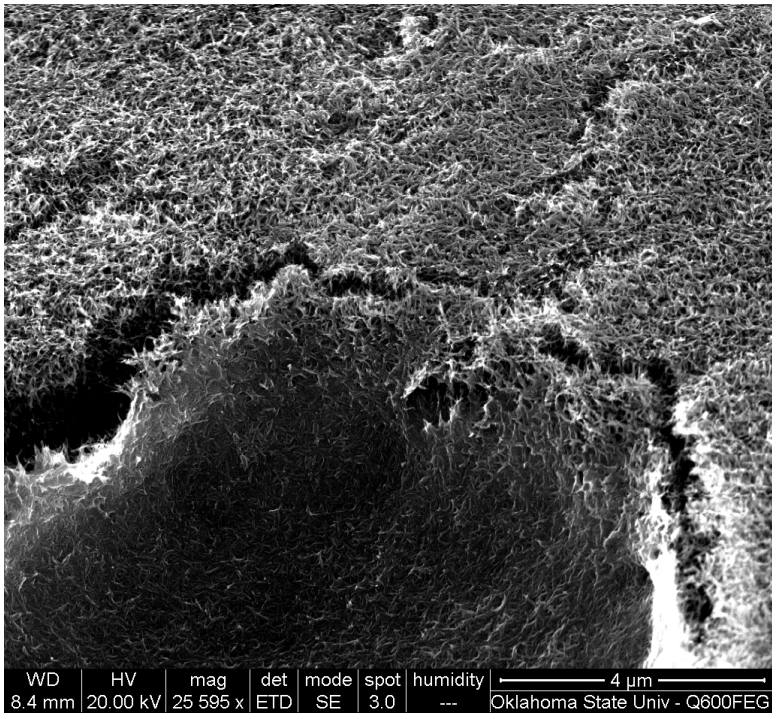

Figure 4.6: Scanning electron microscope image showing the laser exposed region of the vanadia aerogel which is in the lower half of the picture and bordered by the crack.

It has been observed that the same phase transformation occurs in an inert environment. As described in Section 3.4., the transformation in an inert environment was investigated by placing the vanadia aerogel in an optical cell purged with argon. First, the sample was transformed at 6 mW incident power. Subsequently, incident power was decreased to 0.6 mW, and Raman scan was performed and recorded for an accumulation of 200 seconds. As seen in Fig. 4.7, a similar spectrum was observed with an additional peak of 879 cm^{-1}.

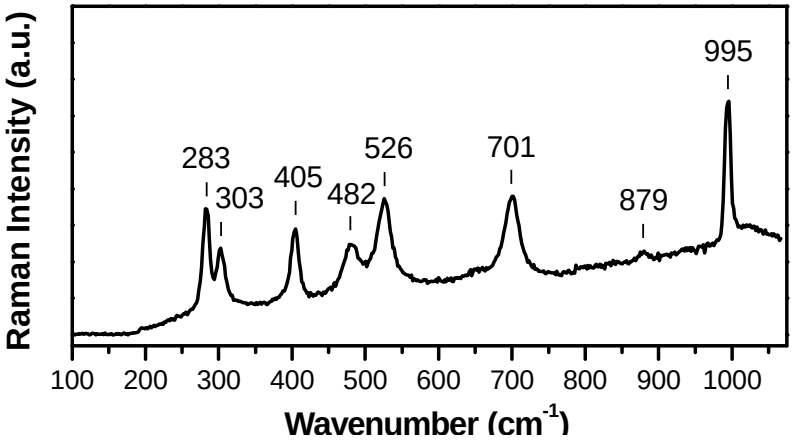

Figure 4.7: Raman spectrum of vanadia aerogel transformed to V_2O_5 in Ar environment.

At first, we associated the 879 cm^{-1} peak with the presence of the inert environment. In particular, we suspected this peak to be a marker of defect creation due to the absence of oxygen in the medium. Since, V_2O_5 contains higher amount of O covalently bonded to V, one expects the transformation consumes O from its environment. Accordingly, the absence of oxygen may prevent establishment of certain V–O bonds leading to the creation of defects. However, later it was observed that the 879 cm^{-1} peak was also observed in air environment when the sample is transformed at low laser irradiation, i.e., around threshold, as the transformation proceeds slowly. However, this peak was observed to be unstable and disappear while the transformation was in progresses. This Raman peak at 879 cm^{-1} is found to identify the presence of H_2O_2 [38]. In particular, it is assigned to O–O stretching in H_2O_2 [38]. Accordingly, the 879 cm^{-1} Raman peak suggests that H_2O_2 is produced as a by-product during the transformation.

The disappearance of the 879 cm^{-1} peak is simply attributed to the instability of H_2O_2, which breaks down to H_2O and O_2.

An interesting feature of the $V_3O_7.H_2O$ to V_2O_5 transformation investigated here is its occurrence at a remarkably low laser intensity (e.g., 0.31 kW/cm^2). This low laser intensity immediately suggests negligible heating effects suggesting the transformation is completely driven optically. In other words, the transformation is expected to be of athermal origin. However, to confirm the athermal nature of the transformation, in situ determination of the temperature during transformation was needed.

As detailed in Section 3.3., this temperature determination was accomplished by Raman spectroscopy. Figure 4.8 shows Stokes and anti-Stokes Raman peaks of vanadia aerogels at laser irradiation close to the threshold for transformation. Raman peaks at ±405 and ±283 cm^{-1} were used for the calculations which are well defined peaks associated with the V_2O_5 phase. The temperature during the transformation was found to be in the range of 25-29 °C.

Although our measurements suggest that the impetus for the $V_3O_7 \cdot H_2O \rightarrow V_2O_5$ transformation is athermal under 514 nm laser radiation, for a rigorous conclusion we also explored thermal conversion of $V_3O_7 \cdot H_2O$ to V_2O_5 by furnace annealing. When the samples were annealed in the furnace, the $V_3O_7 \cdot H_2O \rightarrow V_2O_5$ transformation was observed to take place at around 350 °C. A color change from dark green to yellow was observed indicative of a phase transformation. Figure 4.9 shows the Raman spectrum of the sample after annealing at 350 °C confirming the presence of V_2O_5 and thereby the $V_3O_7 \cdot H_2O \rightarrow V_2O_5$ transformation. In conclusion, this experiment has proven the

athermal nature of the $V_3O_7{\cdot}H_2O \rightarrow V_2O_5$ transformation under 514 nm laser, because the measured temperatures during the transformation separately for laser exposure and furnace annealing cases show a dramatic departure; i.e., 25-29 C vs. 350 °C.

Interestingly, the same $V_3O_7{\cdot}H_2O \rightarrow V_2O_5$ transformation was observed by Zakharova *et al.* in $V_3O_7{\cdot}H_2O$ nanobelt samples annealed at 400 °C [9]. They suggest that the similarity in crystal structures of the two phases (i.e. $V_3O_7{\cdot}H_2O$ andV_2O_5) facilitate the transformation, so that it can occur at 400 °C. They also explain the transformation as a simultaneous dehydration and oxidation of $V_3O_7{\cdot}H_2O$ upon heating that can be expressed in the following equations;

$$V_3O_7 \cdot H_2O \rightarrow V_3O_7 + H_2O \quad (4)$$

$$4V_3O_7 + O_2 \rightarrow 6V_2O_5 \quad (5)$$

In the light-induced transformation investigated by the present thesis, H_2O_2 is likely to be released with H_2O. Alternatively, $V_3O_7{\cdot}H_2O$ may play a catalytic role in transforming H_2O partially to H_2O_2. It is unclear how H_2O_2 is produced and how it impacts the transformation. However, it is likely that the O_2 released from the dissociation of H_2O_2 may facilitate the reaction given by Equation 5 above.

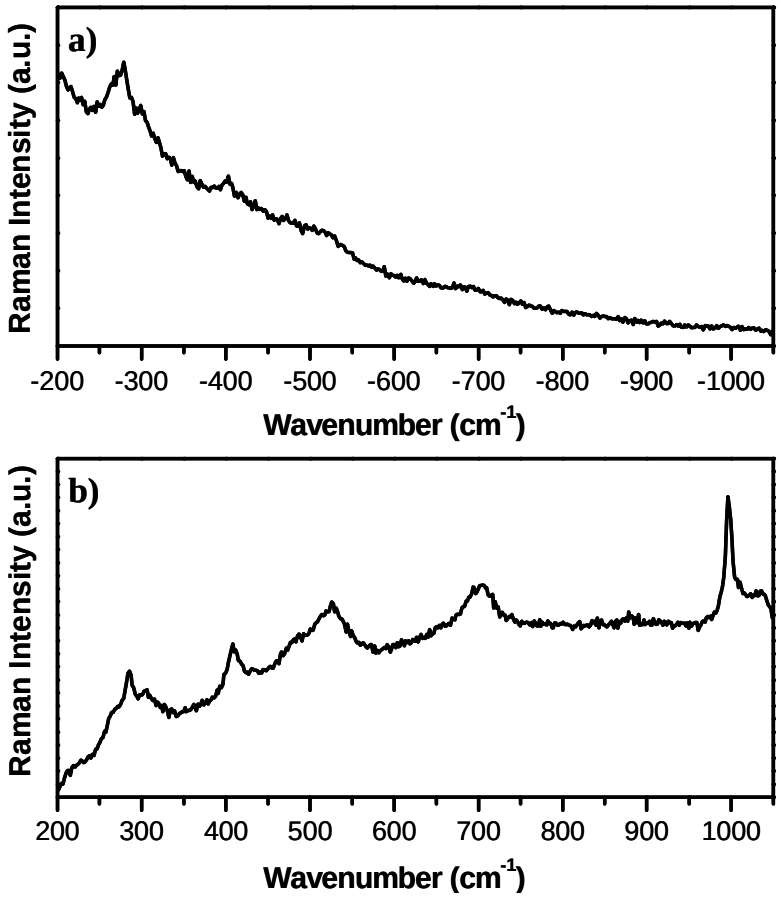

Figure 4.8: a) Anti-Stokes Raman spectrum of semi-transformed vanadia aerogel; **b)** Stokes Raman spectrum of semi-transformed vanadia aerogel.

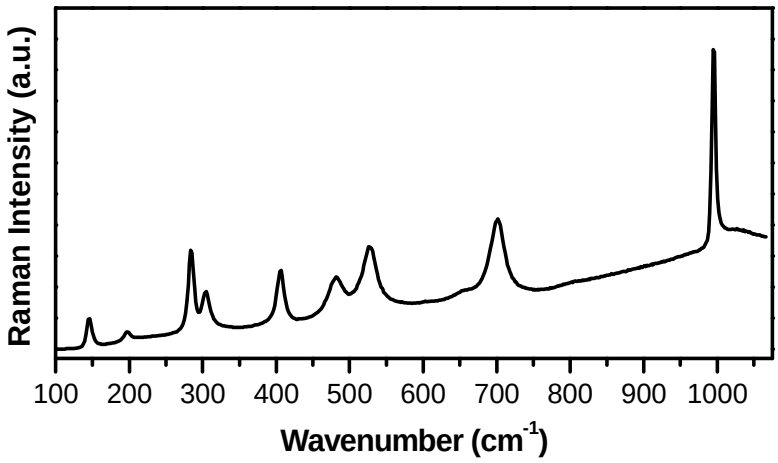

Figure 4.9: Raman spectrum of the aerogel sample after annealing at 350 °C

4.3. Transformation Kinetics by Photoluminescence

As mentioned in Section 3.6, the kinetics of V_3O_7 H_2O to V_2O_5 transformation under laser irradiation was monitored by photoluminescence. Here, one may question why PL was used instead of Raman scattering. Although, high signal to noise Raman spectra of V_2O_5 is obtainable, such a scan at around the threshold laser intensity requires tens of seconds for an acceptable signal to noise. This situation is valid especially at the beginning of the transformation, when the V_2O_5 phase is minor. However, a time resolution of tens of seconds, can not resolve the transformation, which takes about 100 s. This problem cannot be addressed by increasing the laser intensity that increases the transformation rate requiring shorter integration times. Fortunately, the PL of V_2O_5 provides reasonable signal to noise at around the threshold intensity at an integration of 2 s, even at the beginning of the transformation.

Figure 4.10 shows the time evolution PL spectra for a vanadia aerogel sample as it transforms to V_2O_5 at 0 s, 10 s , 20 s, 30 s, 40 s, 60 s, and 100 s. Each spectrum was integrated for 2 s. The time series PL intensity (maximum) in intervals of 2 s is given in Fig. 4.11. The solid line in the plot represents a theoretical fit of the form.

$$I = I_{max}(1 - e^{-at}) \tag{6}$$

where,

I = PL intensity at time t,

I_{max} = Saturation PL intensity,

a = Rate constant.

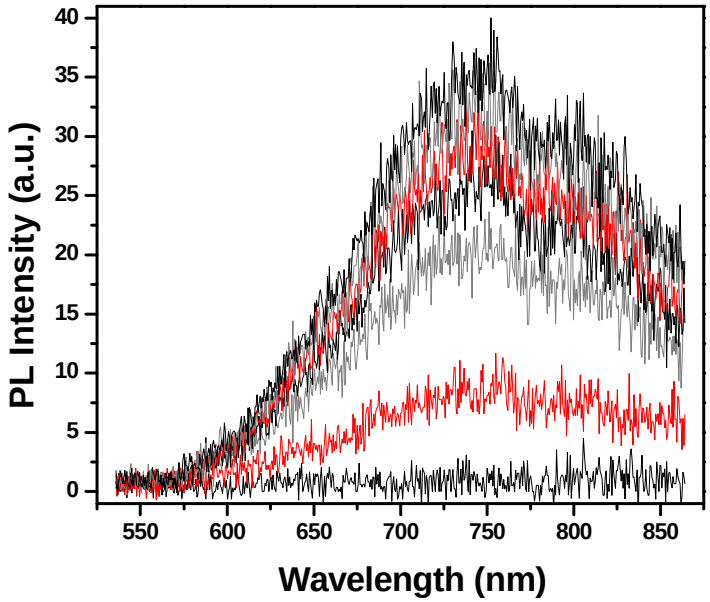

Figure 4.10: PL spectra for vanadium oxide aerogel as it transforms to V_2O_5 captured at 0 s, 10 s, 20 s, 30 s, 40 s, 60 s, and 100 s.

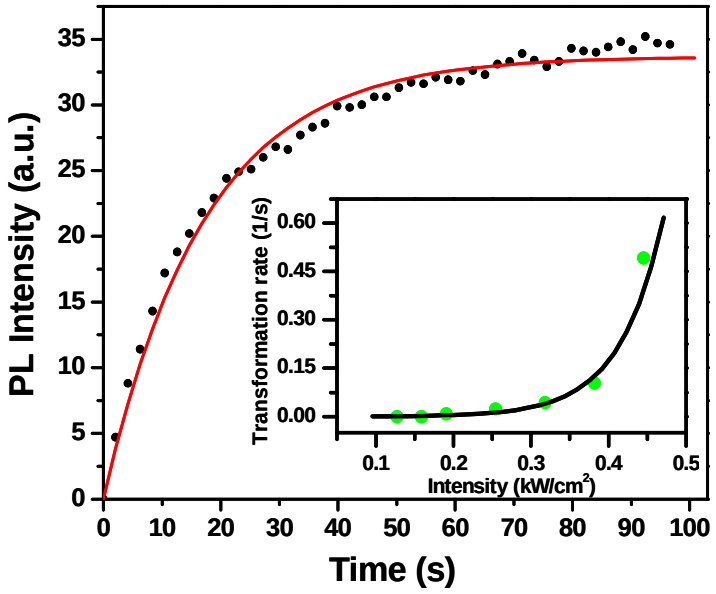

Figure 4.11: Kinetics of V_3O_7 H_2O → V_2O_5 transformation as monitored by PL. Inset shows transformation rate constant as a function of laser intensity.

The relation in Equation 6 is not consistent with nucleation and growth in 2D or 3D. Basically, nucleation and growth occur either by instantaneous nucleation from predetermined nucleation sites, or progressive nucleation where nucleation and growth occur simultaneously [39]. However, in both regimes the initial kinetics should show a superlinear trend due to the increase in the interface between the transformed and untransformed regions. Accordingly, these mechanisms are expected to yield an "S-shaped" kinetics curve that is not observed in the present case. Therefore, two alternative growth models are proposed. An alternative model is that, nucleation occurs at predetermined sites and growth proceeds in 1D. In 1D growth and without progressive nucleation, the interface between the two phases does not increase by time. Rather, the coalescence of the transformed regions eventually decreases the interface area, as the transformation proceeds. This mechanism is consistent with $V_3O_7{\cdot}H_2O$ nanowires, which essentially behave as 1D structural elements. The transformation front in nanowires should move in 1D along the length of the nanowires.

According to the second model, nucleation is not rate limiting and phase transformation occurs as a simple chemical reaction. Equation 6 equivalently argues that the $V_3O_7{\cdot}H_2O$ phase is subject to exponential decay in time: $m(t) = m_o e^{-at}$, where m_o is the initial untransformed mass of $V_3O_7{\cdot}H_2O$ and m(t) is the remaining mass after a transformation time of t. a is the transformation rate constant as defined above. As an example, exponential decay is commonly observed in photobleaching of dye molecules. [40]. The justification for this mechanism could be the removal of an activation barrier for the transformation from $V_3O_7{\cdot}H_2O$ to V_2O_5 under laser excitation due to the proximity

between the structures of the two phases. The athermal nature of the transformation is in accord with this explanation.

The inset in Figure 4.11 shows transformation rate constant, a, as a function of laser intensity. a was derived from the least square fit of kinetics data as in Figure 4.11 to Equation 6 for various laser intensities. Further, a was fit to an exponential relation of the form $a = Ae^{b(I-I_t)}$ where A and b are fitting constants ($A=1.28\times10^{-4}$ and b=5.69 cm^2/kW), I is the laser intensity, and I_t is the threshold laser intensity (0.63 mW).

4.4. Band gap of $V_3O_7{\cdot}H_2O$

Optical absorbance of $V_3O_7{\cdot}H_2O$ is shown in Fig .4.12 for a nanowire concentration of 3.4 g/L in water, from which the band gap was deduced as 1.97 eV. The absorbance is seen to have two regimes: 1) a superlinear regime above a threshold of ≅2 eV which is reminiscent of band to band absorption in a semiconductor; 2) a linear regime below ≅2 eV which is either attributable to subgap absorption due to defects, or a residual phase, or light scattering. Accordingly, the absorbance, A(E), can be fit into the form:

$A(E) = L(E) + C(E - E_g)^n$, where E is the photon energy and L(E) is the linear component. For a semiconductor, optical absorption due to transitions from valence to conduction band is of the form $C(E - E_g)^n$, where E_g is the band gap, and C and n are appropriate constants. As discussed above, L(E) may be fit into a linear relation to a first approximation. In the inset of Fig. 4.12, a semilog plot of A(E) – L(E) is provided which expected to yield an asymptote at E_g, if it obeys a relation of the form $C(E - E_g)^n$.

Clearly, an asymptote is observed at 1.97 eV which is the predicted value for the band gap. Once, L(E) is approximated as linear, Eg may also be clearly predicted from the 1st and 2nd derivatives of A(E). Conducting this analysis E_g is again found to be 1.97 eV. Although, calculation of the band gap involves some approximation here, it is accurate enough to show that $V_3O_7 \cdot H_2O$ has a lower band gap than V_2O_5 by ≅0.5 eV.

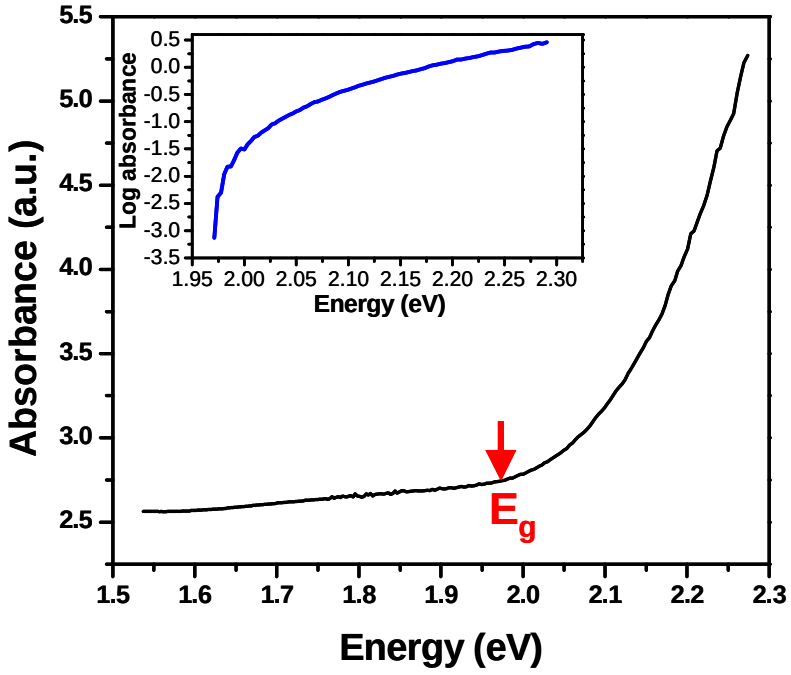

Figure 4.12: Optical absorbance of $V_3O_7 \cdot H_2O$. Inset shows the semilog plot of A(E) – L(E) (where A(E) is the absorbance, and L(E) is the linear part of the absorbance).

CHAPTER 5

CONCLUSIONS AND SUGGESTIONS FOR FUTURE WORK

The following conclusions are drawn from the results of the present thesis work. The author also has suggestions for the advancement of the findings presented so far.

1) A light-induced phase transformation of $V_3O_7 \cdot H_2O$ to V_2O_5 was discovered under 514 nm laser radiation at a remarkably low laser intensity (i.e. as low as 0.31 kW/cm^2).

2) The temperature during the $V_3O_7 \cdot H_2O$ to V_2O_5 transformation was found to be in the range of 25-29 °C that confirms the athermal origin of the transformation.

3) It was observed that the same $V_3O_7 \cdot H_2O$ to V_2O_5 transformation occurs at 350 °C when driven thermally without laser radiation.

4) The light-induced transformation of $V_3O_7 \cdot H_2O$ to V_2O_5 was observed to persist in argon environment under the same conditions suggesting that the transformation can proceed without the presence of oxygen in the surroundings.

5) The appearance and subsequent disappearance of the 879 cm^{-1} Raman peak implies that H_2O_2 is produced as a by-product during the transformation.

6) The transformation kinetics, which fits into the relation $I = I_{max}(1 - e^{-at})$, may be explained by two alternative models: a) nucleation occurs at predetermined sites and growth proceeds in 1D. This mechanism is consistent with $V_3O_7{\cdot}H_2O$ nanowires, which essentially behave as 1D structural elements; b) nucleation is not rate limiting and phase transformation occurs as an ordinary chemical reaction. The justification for this mechanism could be the removal of an activation barrier for the transformation from $V_3O_7{\cdot}H_2O$ to V_2O_5 under laser excitation due to the proximity between the structures of the two phases. The athermal nature of the transformation is in accord with this explanation.

7) Future work must further elucidate the light-induced mechanism of the $V_3O_7{\cdot}H_2O$ to V_2O_5 transformation. In light of Zakharova *et al.,* this transformation is facilitated by the close crystal structures of the two phases that involves minimal conformational changes during the transformation. The impact of the light could be further facilitation of the transformation by elimination of the hydrogen bonds associated with water. The light-induced transformation could be a result of a photocatalytic interaction of VO_6 or VO_5 units with the water already inside the structure.

8) Therefore, termination of hydrogen bonds during the light-driven transformation as well as formation of free water must be investigated by Raman spectroscopy in higher wavenumber range (i.e., 2000-4000 cm^{-1}).

9) The dehydration process during the transformation as well as production of H_2O_2 could be due to the photocatalytic attribute of the $V_3O_7{\cdot}H_2O$. It would be interesting and elucidating to conduct a series of experiments, which involve immersion of $V_3O_7{\cdot}H_2O$ in H_2O_2 in dark as well as in H_2O under laser radiation and monitoring for the transformation and production of H_2O_2, respectively.

BIBLIOGRAPHY

[1] F. D. Chudnovskii, A. L. Pergamet, D. A. Schaefer, and G. B. Stefanovich, "Effect of laser irradiation on the properties of transition metal oxides," *Journal of Solid State Chemistry*, vol. 118, pp. 417-418, 1995.

[2] K. A. Zemski, D. R. Justes, and A. W. Castleman, Jr., "Studies of metal oxide clusters: elucidating reactive sites responsible for the activity of transition metal oxide catalysts," *The Journal of Physical Chemistry B*, vol. 106, pp.6136-6148, 2002.

[3] H. H. Kungm, *Transition metal oxides: surface chemistry and catalysis*. Amsterdam: Elsevier,1989.

[4] A. I. Sidorov, O. P. Vinogradova, V. Yu. Lyubimov, and A. V. Nashchekin, "Synthesis and modification of micro- and nanorods of vanadium oxides," *Technical Physics Letters*, vol. 34, pp. 133–135, 2008.

[5] J. Lappalainen, S. Heinilehto, H. Jantunen, and V. Lantto "Electrical and optical properties of metal-insulator-transition VO_2 thin films," *Journal of Electroceramics*, vol. 22, pp.73-77, 2009.

[6] H. Jerominek, F. Picard, and D. Vincnt, "Vanadium oxide films for optical switching and detection," *Optical Engineering*, vol.32, pp.2092-2099, 1993.

[7] K. Witke, D. Klaffke, A. Skopp, and J. P. Schreckenbach, "Laser-induced transformation as a tool for structural characterization of materials by Raman spectroscopy," *Journal of Raman Spectroscopy*, vol. 29, pp. 411-415, 1998.

[8] Z. Liu, G. Fang, Y. Wang, Y. Bai, and K. Yao, "Laser-induced colouration of V_2O_5," *Journal of Physics D: Applied Physics*, vol. 33, pp. 2327–2332, 2000.

[9] G. S. Zakharova, V. L. Volkov, Ch. Täschner, I. Hellmannb, A. Leonhardt, R. Klingeler, and B. Büchner, "Synthesis and characterization of $V_3O_7{\cdot}H_2O$ nanobelts," *Solid State Communications*, vol. 149, pp. 814-817, 2009.

[10] J. Haber, "Fifty years of my romance with vanadium oxide catalysts," *Catalysis Today*, vol. 142, pp. 100–113, 2009.

[11] B. M. Weckhuysen, and D. E. Keller, "Chemistry, spectroscopy and the role of supported vanadium oxides in heterogeneous catalysis," *Catalysis Today*, vol. 78, pp. 25–46, 2003.

[12] K. Hermann, and M. Witko, "Theory of physical and chemical behavior of transition metal oxides: vanadium and molybdenum oxides," in *The Chemical Physics of Solid Surfaces*, vol. 9, Oxide Surfaces, D.P. Woodruff, Ed. Amsterdam: Elsevier, 2001, pp. 136-198.

[13] P. Balog, D. Orosel, Z. Cancarevic, C. Schön, and M. Jansen., "V_2O_5 phase diagram revisited at high pressures and high temperatures," *Journal of Alloys and Compounds*, vol. 429, pp. 87–98, 2007.

[14] H. P. Wong, B. C. Dave, F. Leroux, J. Harreld, B. Dunn, and L. F. Nazar, "Synthesis and characterization of polypyrrole/vanadium pentoxide nanocomposite aerogels," *Journal of Materials Chemistry*, vol. 8, pp. 1019 – 1027, 1998.

[15] K. Sudoh, and H. Hirashima, "Preparation and physical properties of V_2O_5 aerogel," *Journal of Non-Crystalline Solids*, vol. 147 and 148, pp. 386-388, 1992.

[16] B. Grzybowska-Swierkosz, and F. Trifiro, "Preface," *Catalysis A: General*, vol. 157, pp.1-2, 1997.

[17] D. Manno, A. Serra, M. Di Giulio, G. Micocci, A. Taurino, and A. Tepore, "Structural and electrical properties of sputtered vanadium oxide thin films for applications as gas sensing material," *Journal of Applied Physics*, vol. 81, pp. 2709-2714, 1997.

[18]] S.H. Ng, S.Y. Chewa, J. Wanga, D. Wexler, Y. Tournayre, K. Konstantinov, and H.K. Liu, "Synthesis and electrochemical properties of V_2O_5 nanostructures prepared via a precipitation process for lithium-ion battery cathodes," *Journal of Power Sources*, vol. 174, pp. 1032–1035, 2007.

[19] B. B. Owens, S. Passerini, and W. H. Smyrl, "Lithium ion insertion in porous metal oxides," *Electrochimica Acta*, vol. 45, pp.215-224, 1999.

[20] S. Nishio, and M. Kakihana, "Evidence for visible light photochromism of V_2O_5," *Chemistry of Materials.*, vol. 14, pp. 3730-3733, 2002.

[21] R. J. Colton, A. M. Guzman, and J. W. Abalais, "Photochromism and electrochromism in amorphous transition metal oxide films," *Accounts of Chemical Research.*, vol. 11, pp 170–176, 1978.

[22] F. A. Chudnovskii, A. L. Pergament, D. A. Schaefer and G. B. Stefanovich, "Effect of laser irritation on the properties of transition metal oxides," *Journal of Solid State Chemistry*, vol. 118, pp. 417-418, 1995.

[23] Y. Oka, T. Yao, and N. Yamamoto, "Structure determination of $H_2V_3O_8$ by powder x-ray diffraction," *Journal of Solid State Chemistry*, vol. 89, pp. 372-377, 1990.

[24] Y. Wei , C. Ryub, and K. Kimb, "Improvement in electrochemical performance of V_2O_5 by Cu doping," *Journal of Power Sources*, vol. 165, pp. 386-392, 2007.

[25] O. Šipr, A. Šimůnek, S. Bocharov, Th. Kirchner, and G. Dräger, "Geometric and electronic structure effects in polarized V *K*-edge absorption near-edge structure spectra of V_2O_5," *Physical Review B*, vol. 60, pp. 14115-14127, 1999.

[26] M. F. Al-Kuhaili, E. E. Khawaja, D. C. Ingram, and S. M. A. Durrani, "A study of thin films of V_2O_5 containing molybdenum from an evaporation boat," *Thin Solid Films*, vol. 460, pp. 30-35, 2004.

[27] N. Leventis, C. Sotiriou-Leventis, S. Mulik, A. Dass, J. Schnobrich, A. Hobbs, E. F. Fabrizio, H. Luo, G. Churu, Y. Zhangd and H. Lu, "Polymer nanoencapsulated mesoporous vanadia with unusual ductility at cryogenic temperatures," *Journal of Materials Chemistry*, vol. 18, pp. 2475-2482, 2008.

[28] L. C. Sawyer, D. T. Grubb, and G. F. Meyers, *Polymer Microscopy*, 3rd ed. New York, NY: Springer, 2008.

[29] J. N. Ferraro, K. Nakamoto, and C. W. Brown, *Introductory Raman Spectroscopy*. San Diego, CA: Academic Press, 2002.

[30] E. Smith, and G. Dent, *Modern Raman Spectroscopy*. West Sussex, England: Wiley, 2005.

[31] C. Kittel, *Introduction to Solid State Physics*, 8th ed. Hoboken, NJ: Wiley, 1986.

[32] C.R. Schardt, P. Lucas, A. Doraiswamy, P. Jivaganont, and J. H. Simmons, "Raman temperature measurement during photostructural changes in $Ge_xSe_{1\_x}$ glass," *Journal of Non-Crystalline Solids*, vol. 351, pp.1653–1657, 2005.

[33] H. Harime, T. Hosoda, and S. Nakashima, "Temperature Measurement in a Silicon Carbide Light Emitting Diode by Raman Scattering," *Journal of Electronic Materials*, vol. 28, pp. 141-143, 1999.

[34] JCPDS No: 085-2401, Powder Diffraction File.

[35] C. Sanchez and J. Livage, and G. Lucazeau, "Infrared and raman study of amorphous V_2O_5," *Journal of Raman Spectroscopy*, vol. 12, pp. 68-72, 1982.

[36] W. G. Menezes, D. M. Reis, T. M. Benedetti, M. M. Oliveira, J. F. Soares, R. M. Torresi, and A. J.G. Zarbin , "V_2O_5 nanoparticles obtained from a synthetic

bariandite-like vanadium oxide: Synthesis, characterization and electrochemical behavior in an ionic liquid," *Journal of Colloid and Interface Science*, vol. 337, pp.586-593, 2009.

[37] S. Leea, H. M. Cheong, M. J. Seong, P. Liu, C. E. Tracy,A. Mascarenhas, J. R. Pitts, and S. K. Deb, "Raman spectroscopic studies of amorphous vanadium oxide thin films," *Solid State Ionics*, vol. 165, pp. 111-116, 2003.

[38] S. Ahmad, J. D. McCallum, A. K. Shiemke, and E. H. Appelman, "Raman spectroscopic evidence for side-on binding of peroxide ion to Fe^{III}(edta), *Inorganic Chemistry*, vol 27, pp. 2230-2233, 1988.

[39] J. P. Soto, F. R. Diaz, M. A. del Valle, J.H. Velez, and G.A. East, "Nucleation and growth mechanisms during electropolymerization of substituted 3-alkylthiophenes," *Applied Surface Science*, vol. 254, pp.3489–3496, 2008.

[40] D. L. Kolin, S. Costantino, P. W. Wiseman, "Sampling effects, noise, and photobleaching in temporal image correlation spectroscopy," *Biophysical Journal*, vol.90, pp. 628-639, 2006.

ITA

Çağrı Özge Topal

Candidate for the Degree of

Master of Science

Thesis: Light Induced Transformation of Nanostructured $V_3O_7 \cdot H_2O$ to V_2O_5

Major Field: Mechanical Engineering

Biographical:

Personal Data: Born on November 8, 1984, in Tosya, Kastamonu, Turkey.

Education:

Completed Bachelor of Engineering degree in Mechanical Engineering from Dokuz Eylül University, Izmir, Turkey in May 2006.

Education:

Completed the requirements for the Master of Science in Mechanical Engineering at Oklahoma State University, Stillwater, Oklahoma in May, 2010.

Experience:

Worked as a Research Assistant at Oklahoma State University in Functional Nanomaterials Laboratory.

Name: Çağrı Özge Topal Date of Degree: May 2010

Institution: Oklahoma State University Location: OKC or Stillwater, Oklahoma

Title of Study: Light Induced Transformation of Nanostructured $V_3O_7 \cdot H_2O$ to V_2O_5

Pages in Study: 43 Candidate for the Degree of Master of Science

Major Field: Mechanical Engineering

Scope and Method of Study:
In the present work, light-induced phase transformation of a transition metal oxide has been observed and studied. This phase transformation occurs between two different oxides of vanadium, prepared by sol-gel chemistry, namely from $V_3O_7 \cdot H_2O$ to V_2O_5 under low laser irradiation. Raman scattering was used to monitor the phase transformation and measure the temperature during the transformation. In addition, the kinetics of the phase transformation was probed by photoluminescence. Electron microscopy images and X-ray diffraction data are provided for the elucidation of nanostructure and crystal structure.

Findings and Conclusions:
The $V_3O_7 \cdot H_2O$ to V_2O_5 phase transformation as observed from Raman scattering was found to be occur under laser irradiation as low as $\cong$0.31 kW/cm^2. An interesting feature of this phase transformation is found to be its athermal origin. In addition, the $V_3O_7 \cdot H_2O$ to V_2O_5 transformation was observed to persist in argon environment under the same conditions suggesting that the transformation can proceed without the presence of oxygen in the surroundings. Raman spectroscopy was also employed to rule out the heating effects and measure the temperature during this transformation which is as low as 25-29 °C (i.e., measurements performed at room temperature). In contrast, it was observed that the same transformation occurs at 350 °C when it is driven thermally by annealing samples for 10 minutes. The kinetics of the transformation as measured from photoluminescence suggests 1D nucleation and growth from predetermined nucleation sites. The appearance and subsequent disappearance of the 879 cm^{-1} Raman peak implies that H_2O_2 is produced as a by-product during the transformation.

ADVISER'S APPROVAL: Dr. A. Kaan Kalkan